*DOI:*
10.1002/jmri.26649

*Document Version*
Publisher's PDF, also known as Version of record

# Fast Myocardial $T_1$ Mapping Using Shortened Inversion Recovery Based Schemes

Li Huang, PhD,[1] Radhouene Neji, PhD,[1,2] Muhummad Sohaib Nazir, MD,[1] John Whitaker, MD,[1] Fiona Reid, PhD,[3] Filippo Bosio, BSc,[1] Amedeo Chiribiri, PhD, MD,[1] Reza Razavi, PhD, MD,[1] and Sébastien Roujol, PhD[1]*

**Background:** Myocardial $T_1$ mapping shows promise for assessment of cardiomyopathies. Most myocardial $T_1$ mapping techniques, such as modified Look–Locker inversion recovery (MOLLI), generate one $T_1$ map per breath-held acquisition (9–17 heartbeats), which prolongs multislice protocols and may be unsuitable for patients with breath-holding difficulties.
**Purpose:** To develop and characterize novel shortened inversion recovery based $T_1$ mapping schemes of 2–5 heartbeats.
**Study Type:** Prospective.
**Population/Phantom:** Numerical simulations, agarose/$NiCl_2$ phantom, 16 healthy volunteers, and 24 patients.
**Field Strength/Sequence:** 1.5T/MOLLI.
**Assessment:** All shortened $T_1$ mapping schemes were characterized and compared with a conventional MOLLI scheme (5-(3)-3) in terms of accuracy, precision, spatial variability, and repeatability.
**Statistical Tests:** Kruskal–Wallis, Wilcoxon rank sum tests, analysis of variance, Student's *t*-tests, Bland–Altman analysis, and Pearson correlation analysis.
**Results:** All shortened schemes provided limited $T_1$ time variations (≤2% for $T_1$ times ≤1200 msec) and limited penalty of precision (by a factor of ~1.4–1.5) when compared with MOLLI in numerical simulations. In phantom, differences between all schemes in terms of accuracy, spatial variability, and repeatability did not reach statistical significance ($P > 0.71$). In healthy volunteers, there were no statistically significant differences between all schemes in terms of native $T_1$ times and repeatability for myocardium ($P = 0.21$ and $P = 0.87$, respectively) and blood ($P = 0.79$ and $P = 0.41$, respectively). All shortened schemes led to a limited increase of spatial variability for native myocardial $T_1$ mapping with respect to MOLLI (by a factor of 1.2) ($P < 0.0001$). In both healthy volunteers and patients, the two-heartbeat scheme and MOLLI led to highly linearly correlated $T_1$ times (correlation coefficients ≥0.83).
**Data Conclusion:** The proposed two-heartbeat $T_1$ mapping scheme yields a 5-fold acceleration compared with MOLLI, with highly linearly correlated $T_1$ times, no significant difference of repeatability, and limited spatial variability penalty at 1.5T. This approach may enable myocardial $T_1$ mapping in patients with severe breath-holding difficulties and reduce the examination time of multislice protocols.
**Level of Evidence:** 1
**Technical Efficacy Stage:** 3

J. MAGN. RESON. IMAGING 2019.

Native myocardial longitudinal relaxation time ($T_1$) is sensitive to a wide range of cardiomyopathies.[1] This biomarker is commonly estimated on a per-voxel basis, which is referred to as myocardial $T_1$ mapping.[2] Myocardial $T_1$ maps can also be performed before and after administration of a gadolinium-based contrast agent. The combination of native

View this article online at wileyonlinelibrary.com. DOI: 10.1002/jmri.26649

Received Oct 17, 2018, Accepted for publication Dec 27, 2018.

*Address reprint requests to: S.R., 3rd Floor, Lambeth Wing, St Thomas' Hospital, Westminster Bridge Road, London, SE1 7EH, UK. E-mail: sebastien.roujol@kcl.ac.uk

From the [1]School of Biomedical Engineering and Imaging Sciences, Faculty of Life Sciences and Medicine, King's College London, United Kingdom; [2]MR Research Collaborations, Siemens Healthcare Limited, Frimley, United Kingdom; and [3]School of Population Health and Environmental Sciences, Faculty of Life Sciences and Medicine, King's College London, United Kingdom

Additional supporting information may be found in the online version of this article.

and postcontrast myocardial and blood $T_1$ times enables the estimation of the extracellular volume (ECV) fraction,[3] which has important diagnostic and prognostic value.[4]

A variety of imaging sequences have been proposed for myocardial $T_1$ mapping and often use magnetization preparation pulses such as inversion,[2,5,6] saturation,[7–11] or hybrid pulses.[12,13] In these techniques, a series of images with different $T_1$-weightings is acquired and followed by voxel-wise fitting to a model of the measured signal to generate a $T_1$ map.[2] The modified Look–Locker inversion recovery (MOLLI) sequence[2] and its variations, such as the shortened MOLLI (ShMOLLI)[5] and other modified MOLLI schemes,[16] are inversion recovery based techniques. Although MOLLI $T_1$ times have been shown to be dependent on several parameters including $T_2$,[14,18] magnetization transfer,[19] off-resonance,[16] inversion factor,[20] and heart rate (HR),[16] this approach is commonly used for myocardial $T_1$ mapping due to its high reproducibility/high repeatability, high precision/low spatial variability, and high map quality/low artifact level.[14–17]

Typical MOLLI sequences consist of several inversion pulses, each followed by a series of electrocardiogram (ECG)-triggered single-shot acquisitions. A variety of MOLLI schemes have been proposed using different amounts of $T_1$-weighted images and inversion pulses.[2,5,16] $T_1$ map reconstruction of MOLLI sequences commonly uses a three-parameter (3P) fitting model of the inversion recovery signal[2] followed by a Look–Locker correction.[21] During the fitting process, the signal polarity can be restored using a multifitting approach[2] or a phase-sensitive inversion recovery (PSIR) reconstruction.[22] Alternative MOLLI reconstructions have been proposed using more complex models[23] or Bloch equations simulation of the sequences.[24–26]

The common acquisition manner in MOLLI sequences is a single $T_1$ map per breath-hold, thus limiting the total measurement time. Most MOLLI schemes acquire data over 9–17 heartbeats.[2,5,16] However, breath-holding capabilities may be as low as 2 seconds in patients with cardiac or respiratory disease.[27] Therefore, shortened breath-held acquisition may be beneficial to such patients. Furthermore, the required spatial coverage of myocardial $T_1$ mapping (from single slice to full ventricular coverage) may also depend on the pathology being assessed.[1] MOLLI $T_1$ mapping with full ventricular coverage requires repeated breath-held acquisitions, each for a single slice, thus increasing patient discomfort and prolonging scan time. Therefore, shorter breath-holding requirement for myocardial $T_1$ mapping would be advantageous for multislice $T_1$ mapping protocols.

In this work, we sought to develop and characterize novel shortened inversion recovery based $T_1$ mapping schemes of 2–5 heartbeats.

## Materials and Methods

All imaging was performed using a 1.5T MR scanner (Magnetom Aera, Siemens Healthcare, Erlangen, Germany). This work was conducted according to the Declaration of Helsinki and Good Clinical Practice guidelines and was approved by a local Research Ethics Committee (approval number 01/11/12 for the healthy volunteer study and 15/NS/0030 for the patient study). Informed consent was obtained from all participants.

### $T_1$ Mapping Schemes

Several shortened $T_1$ mapping schemes were evaluated using two, three, four, or five ECG-triggered single-shot images following a single inversion pulse (see Supplementary Material 1). Both magnitude and phase images were reconstructed from these acquisitions. A short inversion time (TI) of $TI_{min}$ = 100 msec was used for the first image.

Two $T_1$ fitting reconstructions using a novel two-parameter (2P) fitting model and a standard 3P fitting model were evaluated. 2P-n ($n$ = 2–5) and 3P-n ($n$ = 3–5), hereafter referred to as $T_1$ mapping using $n$ images following a single inversion pulse with the 2P and 3P fitting models, respectively. These schemes were compared with a conventional 5-(3)-3 MOLLI scheme (i.e., 3P-8). Note that 3P-5 can be seen as an approximation of ShMOLLI for native myocardial $T_1$ mapping.[16]

### $T_1$ Map Reconstruction

*PROPOSED 2P FITTING MODEL.* For $T_1$ fitting, an exhaustive search was performed over a normalized signal dictionary created using the proposed following model:

$$S_{dict}(TI) = 1 - (1 + \delta) \cdot e^{-TI/T_1}, \quad (1)$$

where $\delta \leq 1$ is a constant term representing the inversion factor of the inversion pulse. $\delta$ was determined by Bloch equations simulation of the employed nonselective tuned inversion pulse (phase-modulated hyperbolic tangent, duration 2.56 msec, frequency sweep 9.5 KHz, $\zeta$ = 10, $\tan\kappa$ = 22 with a flip angle of 300°, i.e., a peak $B_1$ strength of 14.4 μT) over typical native and postcontrast myocardial $T_1$ ranges ([400,1600] msec), $B_0$ field inhomogeneity ([–150,+150] Hz), $B_1$ field inhomogeneity ([80%,100%]) and a typical myocardial $T_2$ time of 45 msec.[20] The effective flip angle was approximated based on the average longitudinal magnetization over the slice profile and all simulated $T_1/T_2/B_0/B_1$ regimes. The average inversion factor $\delta$ was estimated as 0.9633. The signal dictionary $S_{dict}(TI)$ was created for a 1-msec-step $T_1$ range of [100,2200] msec, which covers the entire range of native and postcontrast myocardial and blood $T_1$ times.

Before dictionary matching, the polarity-restored measured signal $S_{restored}(TI_j)$ (j = 1,2,…8) was computed from the measured signal $S_{meas}(TI_j)$ (j = 1,2,…8) using a modified PSIR approach. The first image with the shortest TI ($TI_1 = TI_{min}$ = 100 msec), which is one of the only two common images among all schemes, was chosen as the reference phase image with "negative" polarity (i.e., $S_{restored}(TI_1) = -S_{meas}(TI_1)$). Using Bloch equations simulation of the sequence, this assumption was valid for any $T_1$ time > 172 msec (in the presence of any $T_2$ times ≥30 msec and

imaging flip angles ≤85°), thus including the entire physiological ranges of native/postcontrast $T_1$ times in myocardium, blood, and fat (see Supplementary Material 2 for more details). As the signal dictionary is normalized, the polarity-restored measured signal was individually scaled $\left(S_{restored}^{(scaled)}(TI_j)\right)$ to each dictionary entry $S_{dict}(TI_j)$ as:

$$\begin{aligned} S_{restored}^{(scaled)}(TI_j) &= S_{restored}(TI_j) \cdot \frac{\overline{|S_{dict}|}}{\overline{|S_{restored}|}} \\ &= S_{restored}(TI_j) \cdot \frac{\sum_{j=1}^{n} |S_{dict}(TI_j)|}{\sum_{j=1}^{n} |S_{restored}(TI_j)|}, \end{aligned} \quad (2)$$

where n is the amount of $T_1$-weighted images in the 2P-n scheme, $\overline{|S_{dict}|}$ and $\overline{|S_{restored}|}$ are the signal amplitude averages over all TIs ($TI_1$-$TI_n$) of a dictionary entry and the polarity-restored measured signal, respectively. Dictionary matching was finally performed by minimizing the L2-norm between $S_{restored}^{(scaled)}$ and each dictionary entry.

This reconstruction was implemented on an affordable graphics processing unit (GPU) (NVIDIA, Quadro K620 2GB) using the compute unified device architecture (CUDA) to enable high-performance computing. The parallelization level was set to the pixel level. This implementation was compared with a central processing unit (CPU)-only implementation entirely developed in C++. The resulting $T_1$ times were subsequently HR-corrected as described in the second next section.

*3P FITTING MODEL.* The signal of the 3P fitting model is defined as:

$$S(TI) = A - B \cdot e^{-TI/T_1^*}, \quad (3)$$

where A, B, and $T_1^*$ are the model parameters.[2] Note that $T_1^*$ is often referred to as the apparent $T_1$ time. A PSIR reconstruction was employed to restore the signal polarity as described above. A Levenberg–Marquardt solver, provided previously,[28] was used for simultaneous estimation of A, B, and $T_1^*$. $T_1$ times were then approximated as:

$$T_1 = T_1^* \cdot \left(\frac{B}{A} - 1\right), \quad (4)$$

as proposed previously.[2] Finally, a correction for imperfect inversion was performed by dividing $T_1$ times with δ, the inversion factor of the inversion pulse as described above.[20] A subsequent HR correction on the resulting $T_1$ times was performed as described in the next section.

### Heart Rate Correction

Myocardial $T_1$ times using MOLLI have been shown to be HR-dependent.[16,29,30] In this work, a novel approach for correction of HR-dependent $T_1$ errors is proposed for each of the eight evaluated $T_1$ mapping scheme 2P-n ($n$ = 2–5) and 3P-n ($n$ = 3–5) as well as MOLLI. This correction approach was created using phantom experiments in nine agarose/$NiCl_2$ vials with different $T_1/T_2$ times representing typical $T_1/T_2$ ranges of native and postcontrast myocardium and blood (T1MES, Resonance Health, Burswood, WA, Australia). Imaging parameters are described in the next section. The $T_1$ dependence on HR of each $T_1$ mapping scheme is shown in Supplementary Material 3 for each vial. Different linear dependence of measured $T_1$ over physiological HR (40–120 bpm) was observed for different $T_1$ mapping schemes, which is vial- and thus $T_1$-dependent. Individual linear regressions were performed for each $T_1$ mapping scheme and each vial, leading to different slopes and offsets for each $T_1$ mapping scheme and vial (see Supplementary Material 3), as described below:

$$T_1 = \text{slope}(T_1) \cdot HR + \text{offset}(T_1). \quad (5)$$

Note that this relationship is also $T_2$-dependent. Therefore, two different correction models were developed for myocardium (using short-$T_2$ vials with $T_2$~45 msec) and blood (using long-$T_2$ vials with $T_2$ > 150 msec), respectively. Each correction model was created as follows. An empirical method was established to correct the HR-dependent $T_1$ errors by aligning measured $T_1$ times to the value at a theoretical HR of 60 bpm ($T_1^{(corr)}$) based on:

$$\frac{T_1 - \text{offset}(T_1)}{HR} = \frac{T_1 - T_1^{(corr)}}{HR - 60} = \text{slope}(T_1). \quad (6)$$

To make this model applicable to any $T_1$ times (and not limited to the ones corresponding to the phantom), a parabolic relationship between slope, offset, and $T_1$ was empirically defined as:

$$\text{slope}(T_1) = a_1 \cdot [\text{offset}(T_1)]^2 + a_2 \cdot \text{offset}(T_1) + a_3, \quad (7)$$

where $a_1$, $a_2$, and $a_3$ are the coefficients of the parabolic function and were obtained from least square fitting (see Supplementary Material 4). Using Eq. (6), Eq. (7) can then be rewritten as:

$$a_1 \cdot [\text{offset}(T_1)]^2 + \left(a_2 + \frac{1}{HR}\right) \cdot \text{offset}(T_1) + \left(a_3 - \frac{T_1}{HR}\right) = 0. \quad (8)$$

In such case, the offset can be derived as:

$$\text{offset}(T_1) = \frac{1}{2a_1}\left[-\left(a_2 + \frac{1}{HR}\right) \pm \sqrt{\left(a_2 + \frac{1}{HR}\right)^2 - 4 \cdot a_1 \cdot \left(a_3 - \frac{T_1}{HR}\right)}\right], \quad (9)$$

where the positive root (" + " instead of " ± ") was found to provide a physiologically reasonable offset. Then the corrected $T_1$ ($T_1^{(corr)}$) can be computed from Eqs. (6) and (9) as:

$$T_1^{(corr)} = T_1 - \frac{HR - 60}{HR} \cdot [T_1 - \text{offset}(T_1)]. \quad (10)$$

### Experimental Validation

*NUMERICAL SIMULATIONS.* Numerical simulations were used to study the $T_1$ accuracy and precision of the proposed shortened $T_1$ mapping schemes and the conventional 5-(3)-3 MOLLI scheme. The Bloch equations were used to simulate the signal of each sequence by measuring the simulated transverse magnetization at the *k*-space center of each imaging readout. All numerical simulations used a simulated HR of 60 bpm and the following imaging parameters: TR/TE/$TI_1$/$TI_2$ = 2.7/1.1/100/180 msec, 62 phase encoding lines in linear ordering, partial Fourier factor = 7/8, and five start-up pulses. The slice profile of the employed excitation pulse (Hann-filtered sinc pulse without phase modulation, duration 0.48 msec, bandwidth 4660 Hz, time-bandwidth product 1.6, prescribed flip angle 35°, peak strength 10.9 μT) was estimated by Bloch equations simulation over the same $T_1$/$T_2$ ranges and $B_0$/$B_1$ inhomogeneities as used for the inversion pulse. A resulting average excitation flip angle of 26° was obtained and used for the simulations. An average inversion flip angle of 164° corresponding to $\delta = 0.9633$ was also used for the simulations.

Numerical simulations were performed over a range of typical myocardial $T_1$ times (300–1500 msec in steps of 50 msec) and myocardial $T_2$ times (30–70 msec in steps of 5 msec). Monte-Carlo simulation ($N$ = 50,000) were performed for each pair of simulated $T_1$/$T_2$ times using random noise corresponding to a signal-to-noise ratio (SNR) of 50 in the longest-TI image of the conventional MOLLI scheme ($TI_{max}$ = 4100 msec). Accuracy was assessed as the average over the $N$ repetitions of the difference between the simulated and estimated $T_1$ times. Precision was defined as the standard deviation (SD) of the estimated $T_1$ times over the $N$ repetitions.

To evaluate the influence of SNR on $T_1$ accuracy and precision, additional numerical simulations were performed for different SNR ([10,25,50,100]) and $T_1$ range (300–1500 msec in steps of 50 msec), and a fixed $T_2$ times of 45 msec.

*PHANTOM STUDY.* The proposed 2P fitting model was characterized and compared with the conventional 3P fitting model using different shortened $T_1$ mapping schemes and the conventional 5-(3)-3 MOLLI scheme in a phantom with nine agarose/$NiCl_2$ vials of different $T_1$/$T_2$ times in the ranges for native and postcontrast myocardium and blood (T1MES, Resonance Health). To this end, the conventional 5-(3)-3 MOLLI acquisition scheme was used. The first two to five ECG-triggered single-shot images following the first inversion pulse were used for 2P-n ($n$ = 2–5) and 3P-n ($n$ = 3–5). The conventional MOLLI reconstruction using all images (i.e., 3P-8) was also performed. The 2D balanced steady-state free precession (bSSFP) imaging readout used the following parameters: TR/TE/flip angle = 2.7 msec/1.1 msec/35°, field of view (FOV) = 360 × 306 $mm^2$, voxel size = 1.4 × 2.1 $mm^2$, three slices, slice gap = 8 mm, slice thickness = 8 mm, GRAPPA factor = 2, partial Fourier factor = 7/8, bandwidth = 1085 Hz/px, 62 phase-encoding lines in linear ordering, and five start-up pulses.

Experiment #1: Characterization of $T_1$ accuracy, spatial variability, and repeatability. The 5-(3)-3 MOLLI acquisition scheme with a simulated HR of 60 bpm was repeated five times for assessment of $T_1$ accuracy, spatial variability, and repeatability of all schemes. The reference $T_2$ times were obtained from the manufacturer. The reference $T_1$ times were obtained using inversion recovery based spin echo $T_1$ mapping (TI = [50, 100, 200, 300, 400, 500, 600, 700, 800, 900, 1000, 2000, 3000, 4000, 5000] msec, TE/TR = 15/15000 msec). A region of interest (ROI) was manually drawn for each vial. Measured $T_1$ times were obtained for each vial as the averages over the five repetitions of the mean $T_1$ times in the corresponding ROI. $T_1$ accuracy was measured as the difference between measured and reference $T_1$ times. $T_1$ spatial variability was measured for each vial as the average over the five repetitions of the SD of $T_1$ times in the corresponding ROI. $T_1$ repeatability was estimated for each vial as the SD over the five repetitions of the mean $T_1$ times in the corresponding ROI.

Experiment #2: Characterization of the proposed HR correction. The performance of the proposed HR correction was evaluated using a second dataset of measurements where the 5-(3)-3 MOLLI scheme was acquired with different simulated HRs ([40–120] bpm in steps of 10 bpm). All 2P-n and 3P-n reconstructions were performed without and with HR correction using the two different correction models for short-$T_2$ and long-$T_2$ vials. Note that the data used for creating the HR correction models were obtained from a separated study performed earlier on a different day. $T_1$ variation as the average absolute differences with respect to the value at the reference HR of 60 bpm, described as:

$$\text{mean}\{|\Delta_{HR}T_1|\} = \overline{|T_1(HR) - T_1(60)|}, \qquad (11)$$

was calculated for pre- and post-HR-correction on each vial, in order to indicate the $T_1$ mapping sensitivity to HR of each evaluated $T_1$ mapping schemes.

*HEALTHY VOLUNTEER STUDY.* In vivo characterization was performed in 16 healthy volunteers (seven male, 28 ± 3 years). Native myocardial $T_1$ mapping was performed using the 5-(3)-3 MOLLI acquisition scheme and the imaging parameters described in the phantom study. This protocol was modified to acquire three slices in the short axis orientation, each in a separated breath-hold. This acquisition was repeated twice for each healthy volunteer. All 2P-n and 3P-n reconstructions were performed without and with HR correction using the short $T_2$ and long $T_2$-based correction models for myocardial and blood $T_1$ analyses, respectively.

Myocardial $T_1$ analysis was based on a 16-myocardial-segment model,[31] while blood $T_1$ analysis was based on a single ROI drawn inside the left ventricular blood pool in the basal slice with careful exclusion of the papillary muscles. A representative example of ROIs used for myocardial and blood $T_1$ quantification is shown in Supplementary Material 5. All data were visually inspected to detect the presence of severe artifacts or motion among the $T_1$-weighted images. Myocardial segments with apparent severe artifacts in the MOLLI $T_1$ maps were discarded from quantitative myocardial $T_1$ analysis of all schemes. Myocardial and blood $T_1$ times, spatial variability, and repeatability were assessed for each subject. A segment-wise $T_1$ time was calculated as the average over the two repetitions of the $T_1$ mean in each myocardial segment and blood pool. Segment-wise $T_1$ spatial variability was measured as the average over the two repetitions of the $T_1$ spatial SD in each myocardial segment and blood pool. Segment-wise $T_1$ repeatability was estimated as the absolute difference between the two repetitions of the $T_1$ mean in each myocardial segment and blood pool. The corresponding subject-wise $T_1$ time, spatial variability, and repeatability were computed as the averages over all nondiscarded segments, respectively.

*PATIENT STUDY.* Twenty-four consecutive patients (17 male, 53 ± 17 years) referred for clinical cardiac MRI in our center were recruited. Native myocardial $T_1$ mapping was performed in all patients. Eighteen of these patients (13 male, 53 ± 19 years) received an injection of 0.1 mmol/kg of gadobutrol (Gadovist, Bayer Vital, Leverkusen, Germany) as part of the clinical protocols. Postcontrast $T_1$ mapping was thus also performed in these patients. Native and postcontrast myocardial $T_1$ mapping were performed using the same 5-(3)-3 MOLLI acquisition scheme and imaging parameters described in the healthy volunteer study. Three slices were acquired in the short axis orientation, each in a separated breath-hold. All 2P-n and 3P-n reconstructions were performed without and with HR correction using the short $T_2$ and long $T_2$-based correction models for myocardial and blood $T_1$ analyses, respectively. Subject-wise myocardial and blood $T_1$ times were measured as described in the healthy volunteers section.

### Statistical Analysis

Kruskal–Wallis test and a one-way analysis of variance (ANOVA) test were used to compare all $T_1$ mapping schemes in phantom and in vivo, respectively. A result was considered statistically significant at the 5% significance level (i.e., $P < 0.05$) and all tests were two-tailed. When the Kruskal–Wallis or one-way ANOVA test demonstrated statistical significance, Wilcoxon rank sum tests or Student's *t*-tests were performed for each pair of $T_1$ mapping schemes using Bonferroni correction, which resulted in a statistical significance threshold of $0.05/C_8^2 \approx 0.0018$. Correlation and agreement analyses in the form of Pearson correlation analysis and Bland–Altman plots with limits of agreement, respectively, were performed between each shortened $T_1$ mapping scheme and MOLLI in terms of subject-wise native/postcontrast myocardial/blood $T_1$ times. Bland–Altman limits of agreement were calculated as the mean difference between methods (also called bias) ± 1.96 × (SD of differences); ~95% of differences between methods should lie within these limits.

## Results

### Computational cost of the 2P model-based reconstruction

2P-2, 2P-3, 2P-4, and 2P-5 reconstruction times for one $T_1$ map (256 × 256 matrix size) were 7, 8, 11, and 13 seconds using a CPU-based implementation, respectively. These reconstruction times were reduced to 0.2 seconds for all 2P reconstructions using the proposed GPU-based implementation. Reconstruction times for all CPU-based implementations increased linearly with the number of slices, while GPU-based reconstruction times increased at a slower rate. For example, 2P-2, 2P-3, 2P-4, and 2P-5 reconstruction times for 10 $T_1$ maps (256 × 256 × 10 matrix size) were 65, 83, 104, and 130 seconds using the CPU-based implementation, and were reduced to 1, 1.3, 1.7, and 2 seconds using the proposed GPU-based implementation, respectively.

### Numerical Simulations

Accuracy and precision of all evaluated $T_1$ mapping schemes are shown in Fig. 1. All 3P-n schemes led to limited $T_1$ time variation (≤2%) with respect to MOLLI for the entire range of $T_1$ times ([300,1500] msec). All 2P-n schemes provided limited $T_1$ time variations (≤2%) with respect to MOLLI for $T_1$ times ≤1200 msec but resulted in reduced accuracy for longer $T_1$ times. All shortened $T_1$ mapping schemes led to a precision penalty with respect to MOLLI by a factor of ~1.4–1.5. All studied schemes were $T_2$-dependent. Lower $T_2$ times were associated with decreased accuracy for all schemes.

SNR had limited influence on the $T_1$ time estimates of all schemes (variation ≤2% with respect to $T_1$ estimations with an SNR of 100, see Supplementary Material 6). Lower SNR resulted in a reduced $T_1$ precision of all schemes. However, SNR had limited influence on the relative precision penalty of all shortened $T_1$ mapping schemes with respect to MOLLI, which was by a factor of 1.4–1.5 for the entire SNR range.

### Phantom Study

Experiment #1: Characterization of $T_1$ accuracy, spatial variability, and repeatability. $T_1$ accuracy, spatial variability, and repeatability in phantom using all evaluated $T_1$ mapping schemes (conventional MOLLI and shortened $T_1$ mapping schemes: 2P-n [$n$ = 2–5] and 3P-n [$n$ = 3–5]) are shown in Fig. 2. All schemes were in good agreement with the reference $T_1$ times for long-$T_2$ vials (i.e., $T_2$ > 150 msec) with an

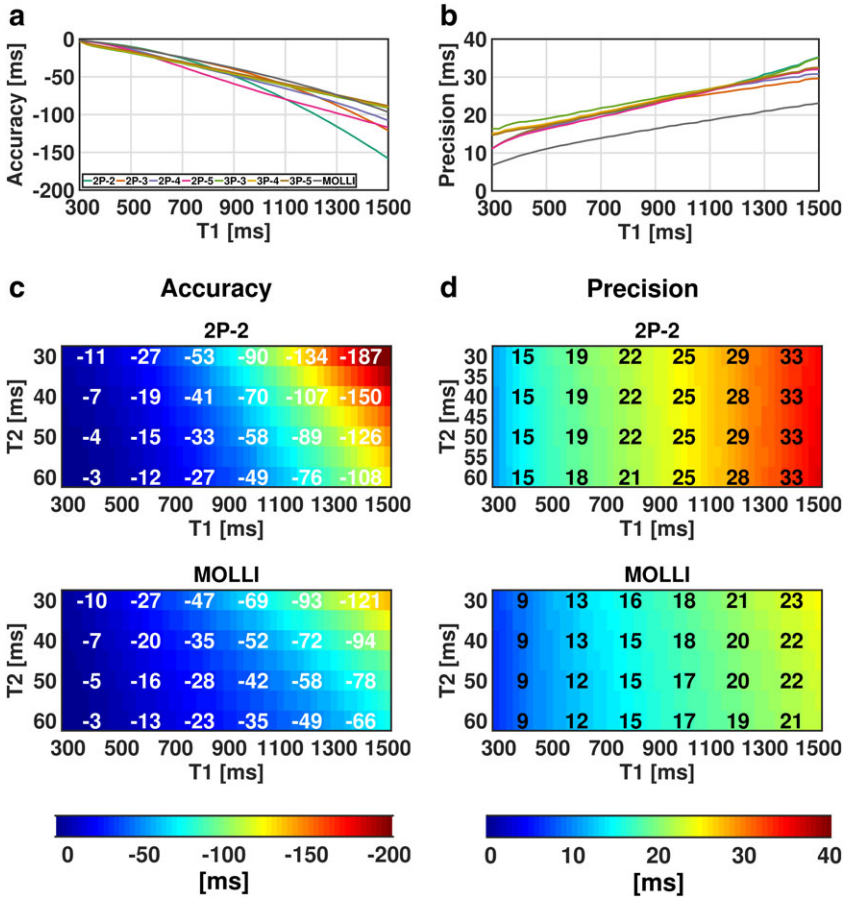


**FIGURE 1: Numerical simulations of $T_1$ accuracy and precision of all $T_1$ mapping schemes. $T_1$ accuracy (a) and precision (b) are shown as a function of $T_1$ using a typical myocardial $T_2$ time of 45 msec for all $T_1$ mapping schemes. Impact of $T_2$ times on $T_1$ accuracy (c) and precision (d) are shown for 2P-2 and MOLLI.**

average error of <11 msec for all schemes. All schemes led to underestimated $T_1$ times for short-$T_2$ vials (i.e., $T_2$~45 msec) with respect to the reference $T_1$ times. Although MOLLI tended to provide slightly lower underestimation than shortened $T_1$ mapping schemes (especially for short-$T_2$ vials), these differences were not statistically significant ($P$ = 1.00). For a typical native myocardial $T_1$ range (the vial with $T_1/T_2$ 1160/48 msec), 2P-2 and 2P-5 led to an underestimation of 25 msec and 22 msec with respect to MOLLI, while the other shortened $T_1$ mapping schemes led to an underestimation of <10 msec. The 2P-n ($n$ = 2–5) schemes tended to provide lower spatial variability than the 3P-n ($n$ = 3–5) schemes for typical postcontrast $T_1$ range (<450 msec), while 2P-2 and 3P-3 tended to show higher spatial variability than other schemes for long $T_1$ times (>1400 msec). Although all schemes tended to provide higher spatial variability than MOLLI (7–8 msec vs. 5 msec, respectively), and lower repeatability than MOLLI (1.2–1.5 msec vs. 1.0 msec, respectively), these differences were not statistically significant ($P$ = 0.71 and $P$ = 0.75, respectively).

Experiment #2: Characterization of the proposed HR correction. Supplementary Material 7 shows the impact of the proposed HR correction for measured $T_1$ times. After the proposed HR correction, $T_1$ variation over all HR was reduced from a maximum of 55 msec to a maximum of 7 msec for all vials and $T_1$ mapping schemes.

### *Healthy Volunteer Study*

Example native myocardial $T_1$ maps of a healthy volunteer using all $T_1$ mapping schemes are shown in Fig. 3. All schemes provided similar visual image quality across all slices and segments, as well as similar native $T_1$ ranges for myocardium and blood. The perceived noise, however, was higher in the left ventricular blood pool for all shortened $T_1$ mapping schemes.

The average HR over all healthy volunteers was 68 ± 12 bpm (51–90 bpm). On average, over all healthy volunteers, the magnitude of HR correction for native myocardium ranged from 0.03 ± 0.05 msec (≤0.17 msec) using 2P-5 to 12 ± 9 msec (≤30 msec) using 2P-2, while the magnitude of HR correction for native blood ranged from 3 ± 2 msec (≤8 msec) using 2P-5 to 14 ± 12 msec (≤41 msec) using 2P-2.

Over all healthy volunteers, only one of 256 myocardial segments (0.4%) was discarded from the analysis. There were no statistically significant differences between all schemes in terms of native myocardial $T_1$ times ($P$ = 0.21), which were all in the range of 977–997 msec (Fig. 4a). There were no statistically significant differences between all shortened $T_1$

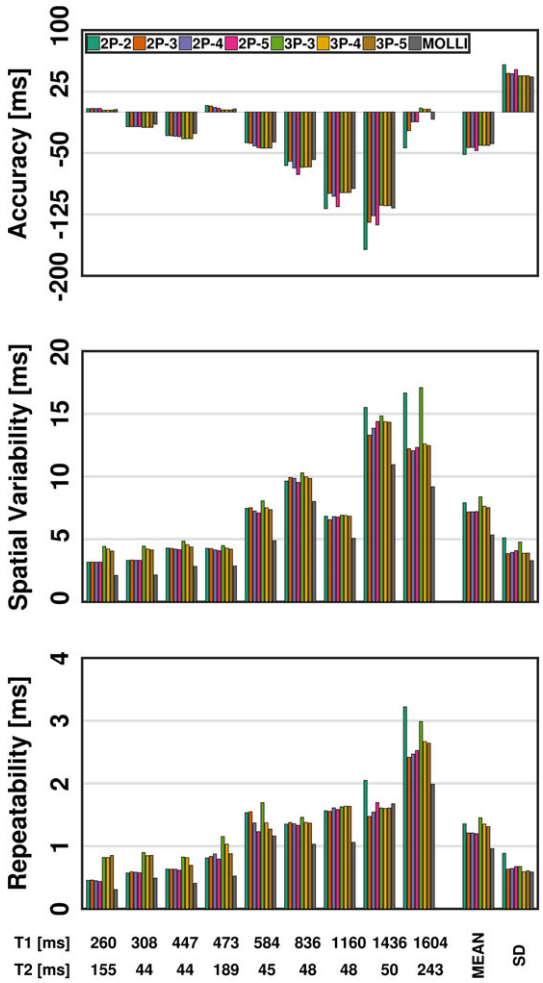


**FIGURE 2: $T_1$ accuracy (a), spatial variability (b), and repeatability (c) of all $T_1$ mapping schemes in phantom experiments. There were no statistically significant differences between all schemes in terms of accuracy ($P$ = 1.00), spatial variability ($P$ = 0.71) and repeatability ($P$ = 0.75).**

mapping schemes in terms of myocardial $T_1$ spatial variability ($P$ = 0.87). However, they all had increased spatial variability by a factor of 1.2 with respect to MOLLI (56–59 msec vs. 48 msec, respectively, $P$ < 0.0001) (Fig. 4b). There were no statistically significant differences between all schemes in terms of myocardial $T_1$ repeatability, which were in the range of 14–18 msec ($P$ = 0.87) (Fig. 4c).

Over all healthy volunteers, no statistically significant differences were found between all schemes in terms of native blood $T_1$ times, which were in the range of 1583–1623 msec ($P$ = 0.79) (Fig. 4d). 2P-2 and 3P-3 yielded higher spatial variability in the blood pool (85 msec and 105 msec, respectively) than the other shortened $T_1$ mapping schemes (63 msec, $P \leq 0.0025$), which were all inferior to MOLLI (49 msec, $P$ < 0.0001) (Fig. 4e). There were no statistically significant differences between all schemes in terms of repeatability of native blood $T_1$ times ($P$ = 0.41), which were in the range of 7–15 msec for all schemes (Fig. 4f).

Segment-wise assessment of native myocardial $T_1$ times, spatial variability, and repeatability of 2P-2 and MOLLI are shown in Fig. 5. The segmental variation (SD over all myocardial segments) of native myocardial $T_1$ times, spatial variability, and repeatability was of similar range between 2P-2 and MOLLI [13/6/3 msec vs. 12/8/3 msec, respectively]).

### *Patient Study*

Example native and postcontrast myocardial $T_1$ maps obtained in two patients using all the evaluated $T_1$ mapping schemes are shown in Figs. 6 and 7, respectively. Similar visual image quality and native myocardial $T_1$ range were obtained for all schemes, although a higher perceived noise level can be observed in the left ventricular blood pool using shortened $T_1$ mapping schemes.

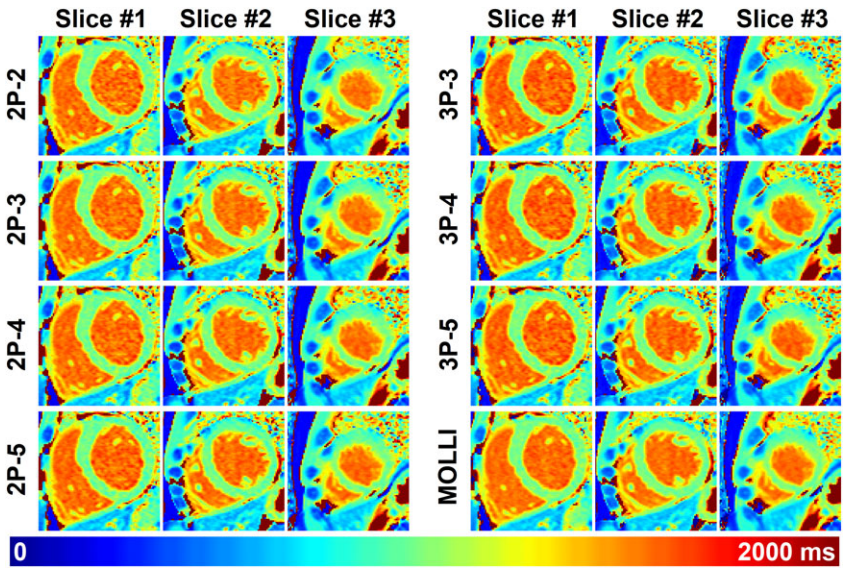


**FIGURE 3: Example native $T_1$ maps of a 29-year-old male healthy volunteer (HR 52 bpm) along the short axis using all $T_1$ mapping schemes. Similar image quality and native $T_1$ range were obtained across all slices using all schemes.**

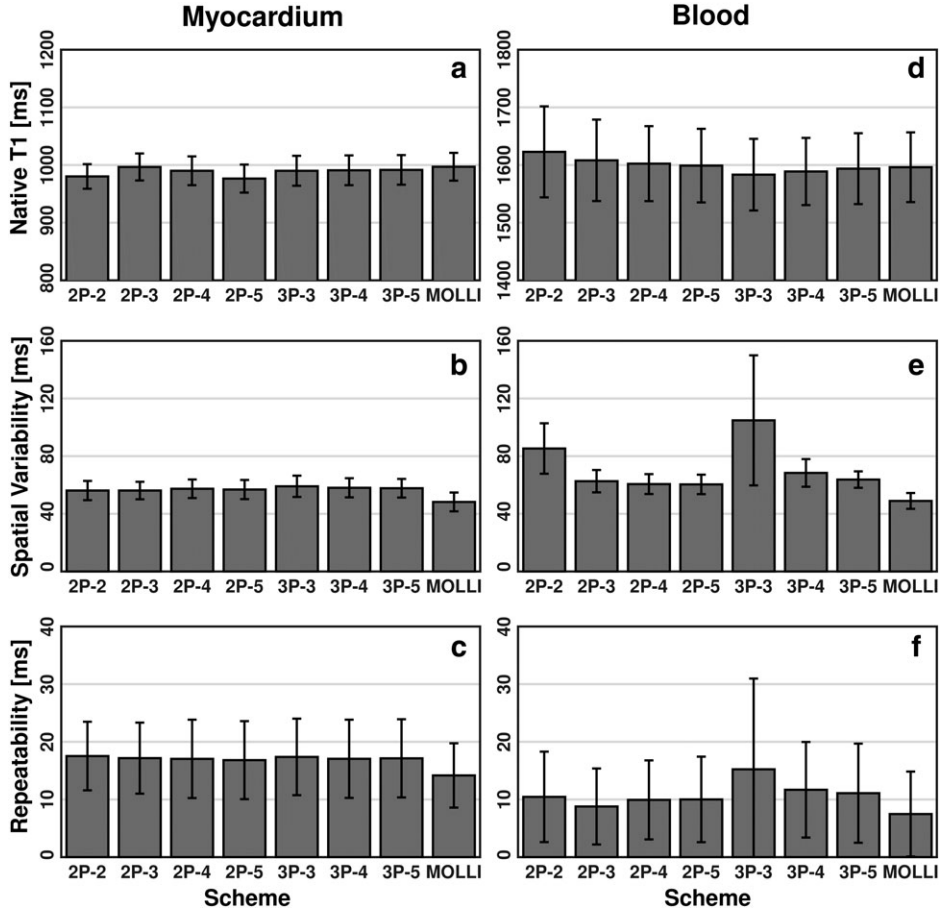


**FIGURE 4: Native $T_1$ times, spatial variability, and repeatability for myocardium (a–c, respectively) and blood (d–f, respectively) obtained using all $T_1$ mapping schemes in 16 healthy volunteers. Average (bar plots) and SD (error bars) over all healthy volunteers are presented. There were no statistically significant differences between native myocardial and blood $T_1$ times ($P = 0.21$ and $P = 0.79$, respectively) and repeatability ($P = 0.87$ and 0.41, respectively) obtained using all schemes. All shortened $T_1$ mapping schemes led to increased myocardial and blood $T_1$ spatial variability with respect to MOLLI ($P < 0.0001$).**

Over all patients, the average HR was 68 ± 14 bpm (36–98 bpm). In all, 34 of 384 myocardial segments (9%) from five patients for native $T_1$ mapping and 11 of 288 myocardial segments (4%) from two patients for postcontrast $T_1$ mapping were discarded from the quantitative analysis due to substantial artifacts and/or motion. HR correction of native myocardial $T_1$ times led to changes from 0.04 ± 0.06 msec (≤0.25 msec) using 2P-5 to 13 ± 12 msec (≤43 msec) using 2P-2, while HR correction of native blood $T_1$ times led to changes from 3 ± 3 msec (≤11 msec) using 2P-5 to 14 ± 13 msec (≤47 msec) using 2P-2. The magnitude of HR correction for postcontrast myocardial and blood $T_1$ times was <4 msec using all schemes.

Subject-wise native and postcontrast $T_1$ times for myocardium and blood using all schemes are shown in Fig. 8. There were no statistically significant differences between all schemes for each of these four $T_1$ ranges (native/postcontrast myocardial/blood) ($P \geq 0.19$).

The Pearson correlation and Bland–Altman analyses in terms of subject-wise native myocardial/blood $T_1$ times (healthy volunteers and patients) and postcontrast myocardial/-blood $T_1$ times (patients only) are shown in Fig. 9 (only 2P-2 vs. MOLLI) and Table 1 (each shortened scheme vs. MOLLI). Strong correlation was observed between 2P-2 and MOLLI. The Pearson correlation coefficient between 2P-2 and MOLLI for native blood $T_1$ times was 0.83, and was ≥0.96 for all other $T_1$ ranges. All other shortened $T_1$ mapping schemes were also strongly correlated with MOLLI for each $T_1$ range (Pearson correlation coefficient ≥ 0.90). For native blood $T_1$ times, 2P-2 and MOLLI were in moderate agreement (bias of 40 msec, 95% limits of agreement: –51 msec to 130 msec). For other $T_1$ ranges, 2P-2 and MOLLI were in good agreement with limited bias magnitude (≤17 msec) and narrow width of 95% limits of agreement (<43 msec). All other shortened $T_1$ mapping schemes were in good agreement with MOLLI for native myocardial $T_1$ mapping, with limited bias magnitude (≤19 msec) and narrow width of 95% limits of agreement (<39 msec).

Supplementary Material 8 shows native myocardial $T_1$ maps obtained in a patient who was unable to sustain a stable breath-hold for the entire duration of the acquisition. MOLLI led to substantial $T_1$ map artifacts in both mid-ventricular and apical slices, which were then discarded for all

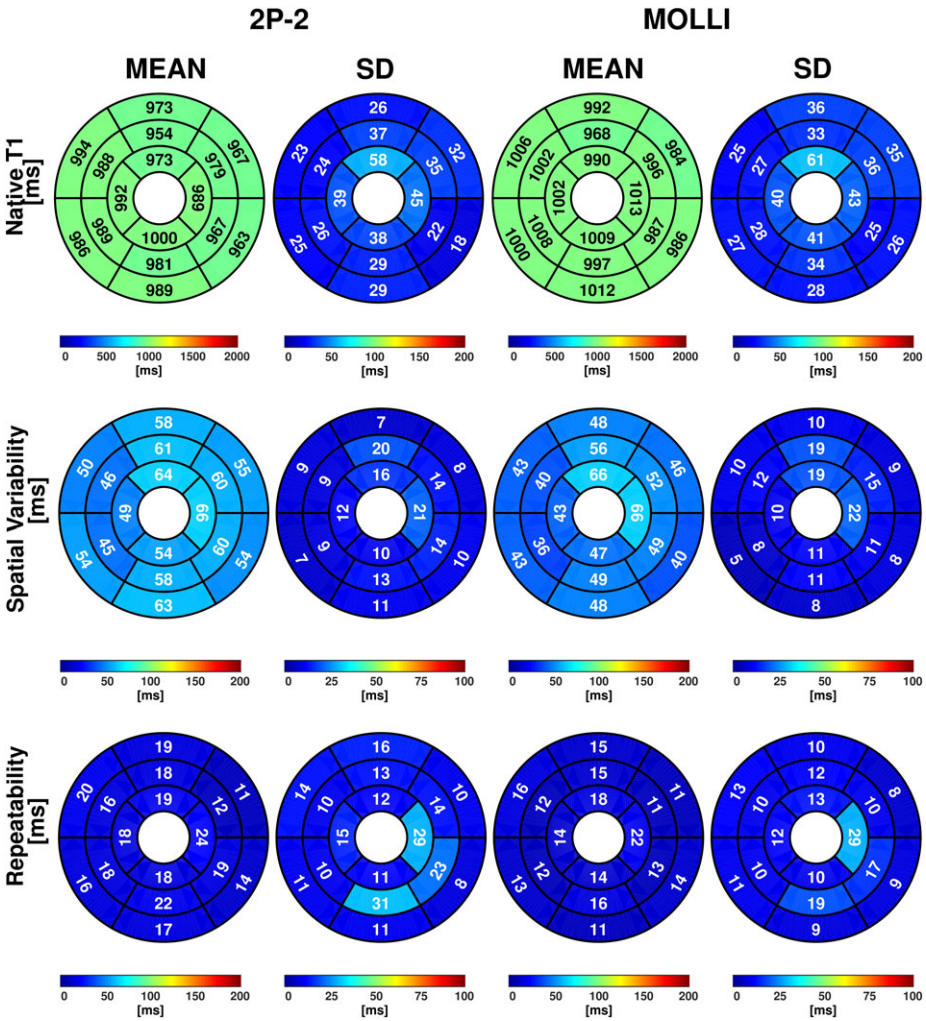


FIGURE 5: Segment-wise native myocardial $T_1$ times, spatial variability, and repeatability using 2P-2 and MOLLI in 16 healthy volunteers. Data are shown as average $\pm$ SD over all healthy volunteers. No statistically significant differences were found between segmental values of native $T_1$ times, spatial variability, and repeatability obtained using both methods.

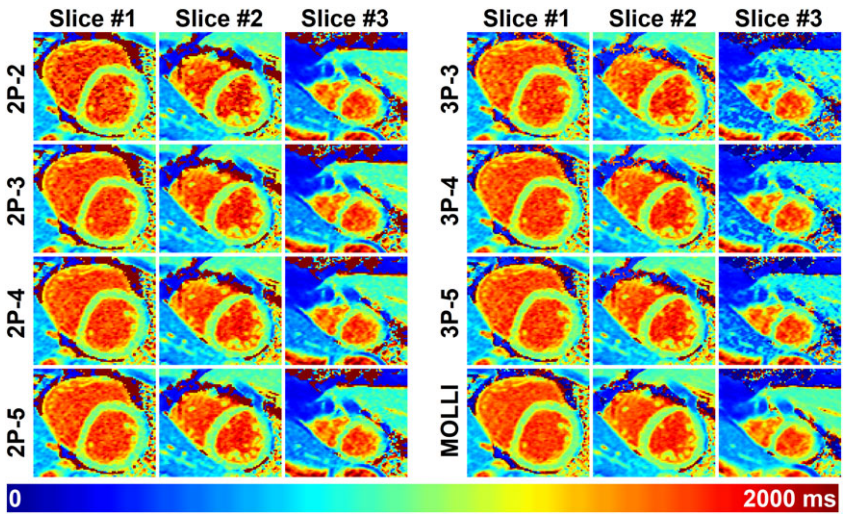


FIGURE 6: Example native myocardial $T_1$ maps of a 38-year-old male patient (HR 84 bpm) admitted with syncope using all $T_1$ mapping schemes. All schemes provided similar $T_1$ map image quality and similar characteristics for native myocardial $T_1$ times. Shortened schemes tended to have lower spatial homogeneity than MOLLI in the blood pool.

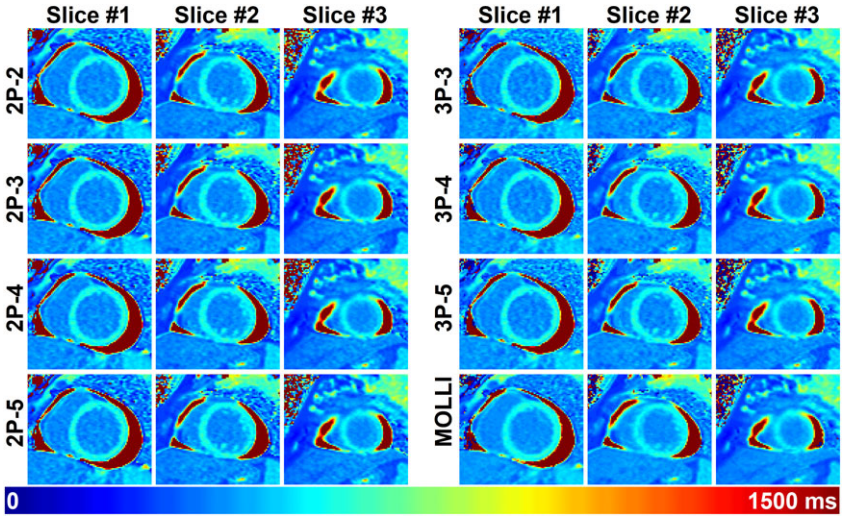


**FIGURE 7: Example postcontrast myocardial $T_1$ maps obtained in a 32-year-old female patient (HR 61 bpm) with severe left ventricular systolic dysfunction and pericardial effusion using all $T_1$ mapping schemes. All schemes provided similar $T_1$ map image quality as well as similar myocardial and blood $T_1$ ranges across all slices.**

schemes from the quantitative analysis. All shortened $T_1$ mapping schemes provided improved map quality in this patient.

## Discussion

In this work, we proposed and evaluated shortened $T_1$ mapping schemes combined with a novel 2P fitting model for myocardial $T_1$ mapping. These methods were successfully evaluated in numerical simulations, phantom, healthy volunteers, and patients. Compared with the conventional MOLLI 5-(3)-3 scheme, shortened $T_1$ mapping schemes (down to two heartbeats only) combined with the proposed 2P fitting model resulted in no significant differences in terms of $T_1$ estimates and repeatability and had similar $T_1$ ranges as well as limited reduction of precision/increase of spatial variability. Importantly, the resulting native/postcontrast myocardial/blood $T_1$ times measured by all shortened $T_1$ mapping schemes were highly linearly correlated with the corresponding values measured using MOLLI. Finally, the proposed GPU implementation of the exhaustive search-based optimization of the 2P fitting model enables fast $T_1$ map reconstruction, which is suitable for clinical application.

In vivo myocardial $T_1$ times, precision, and repeatability of MOLLI were in good agreement with previous works.[6,14,32] All evaluated shortened $T_1$ mapping schemes provided $T_1$ times

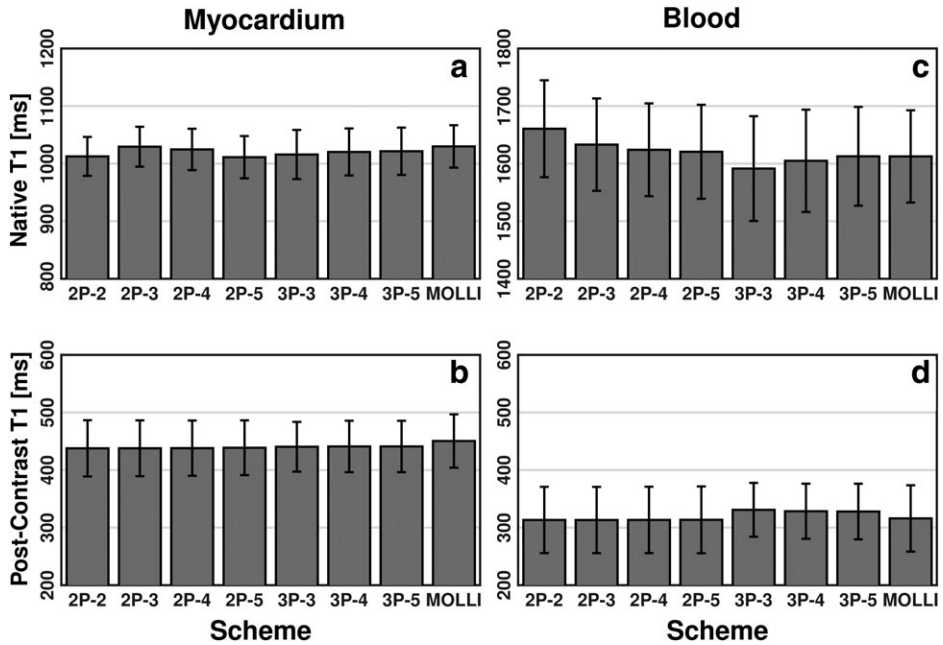


**FIGURE 8: Native/postcontrast myocardial/blood $T_1$ times (a–d, respectively) in 24 patients using all $T_1$ mapping schemes. Average (bar plots) and SD (error bars) over all patients are presented. All methods led to similar range of native/postcontrast myocardial/blood $T_1$ times ($P \geq 0.19$).**

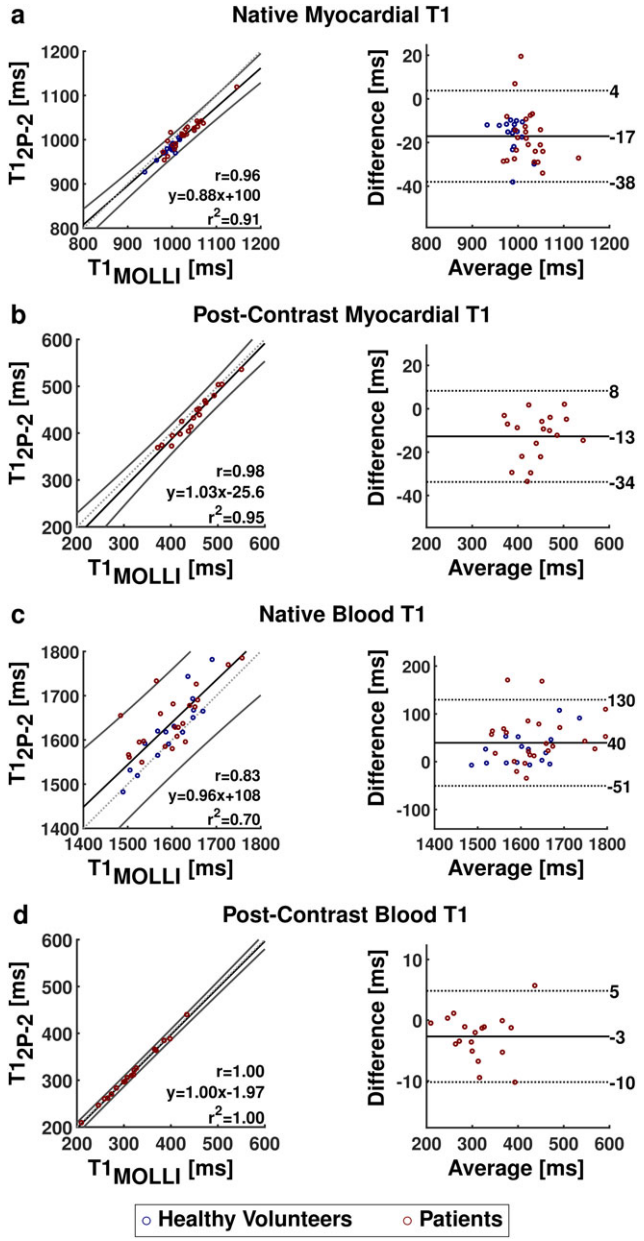


**FIGURE 9: Correlation and agreement tests between $T_1$ times obtained using 2P-2 and MOLLI in all subjects including 16 healthy volunteers and 24 patients. Subfigure (a–d) illustrate Pearson correlation analysis and Bland–Altman plot of native myocardial $T_1$ times, native blood $T_1$ times, postcontrast myocardial $T_1$ times, and postcontrast blood $T_1$ times, respectively. Strong correlation and good agreement were found between $T_1$ times obtained using 2P-2 and MOLLI. In Pearson correlation analysis plots, confidence interval (solid lines) and identity line (y = x, dashed line) are also plotted besides the linear regression line (solid line). Correlation information including the Pearson correlation coefficient (r-value), linear regression relationship (y as a function of x), and coefficient of determination ($r^2$) is also displayed in Pearson correlation plots. In Bland–Altman plots, "average" stands for $(T1_{2P\text{-}2} + T1_{MOLLI})/2$ and "difference" stands for $(T1_{2P\text{-}2}\text{-}T1_{MOLLI})$.**

in a similar range as MOLLI for all native/postcontrast myocardial/blood $T_1$ ranges. Moreover, all proposed shortened $T_1$ mapping schemes have the same acquisition manner as 5-(3)-3 MOLLI. These observations suggest that, similar to MOLLI, these shortened $T_1$ mapping schemes are also sensitive to $T_2$ relaxation,[14,18] magnetization transfer,[19] and off-resonance effects.[16] Furthermore, this work was performed at 1.5T. The potential of these shortened $T_1$ mapping schemes at higher fields such as 3T remains to be demonstrated and will be the focus of future work.

The feasibility of the shortened $T_1$ mapping schemes for postcontrast myocardial $T_1$ mapping was demonstrated in numerical simulations, phantom, and patients. The spatial variability penalty of shortened $T_1$ mapping schemes was more pronounced for typical short postcontrast $T_1$ times than typical native myocardial $T_1$ times, which could be interpreted as a consequence of lacking a second short-TI image. For short $T_1$ times (i.e., typical postcontrast $T_1$ times), all 2P-n schemes had higher precision and lower spatial variability than the shortened 3P-n schemes. Therefore, 2P-n schemes may be advantageous over shortened 3P-n schemes in the context of ECV mapping.

The healthy volunteer study demonstrated that all proposed shortened $T_1$ mapping schemes resulted in an increase of $T_1$ spatial variability (by a factor of 1.2) for native myocardial $T_1$ times when compared with MOLLI. This increase in spatial variability between 3P-5 (approximated ShMOLLI for native $T_1$) and MOLLI is in good agreement with previous comparison of ShMOLLI and MOLLI at 1.5T.[5] Importantly, the use of fewer images for both 2P-n and 3P-n (i.e., $n$ = 2/3/4) did not result in a further increase of spatial variability (i.e., precision loss) of native myocardial $T_1$ time estimates when compared with 3P-5. This suggests that the impact of each $T_1$-weighted image in the fitting process is dependent on its corresponding TI, similar to findings observed for saturation recovery-based techniques.[33,34] Long TI images (i.e., with TI >> $T_1$ range of interest) have reduced $T_1$-weighted contrast and may thus have reduced contributions to the precision of $T_1$ estimates.

For long $T_1$ times such as in vivo native blood $T_1$ times, 2P-2 led to a larger increase of spatial variability by a factor of 1.7 with respect to MOLLI, while other 2P-n schemes still maintained a limited increase of $T_1$ spatial variability by a factor < 1.28. This could be explained by the lack of sampling of long TI times in the 2P-2 scheme. Therefore, 2P-3 could be a valuable alternative to 2P-2 for native $T_1$ mapping, as it offers lower spatial variability for blood $T_1$ quantification. However, blood $T_1$ time is usually measured as the spatial average over a large ROI, which may mitigate this effect for 2P-2, as no statistically significant differences were found in terms of repeatability for blood $T_1$ quantification among all methods.

Myocardial $T_1$ mapping based on the acquisition of only two images has been previously proposed using the AIR technique, which is based on saturation recovery.[9] However, this technique was shown to considerably increase spatial variability of native myocardial $T_1$ mapping by a factor of 2.5 when compared with MOLLI.[35] The proposed 2P-2

**TABLE 1. Pearson Correlation Analysis and Bland–Altman Plot Results**

| | Native myocardial T1 | Native blood T1 | Postcontrast myocardial T1 | Postcontrast blood T1 |
|---|---|---|---|---|
| 2P-2 | 0.96 | 0.83 | 0.98 | 1.00 |
| | –17 ± 11 (–38,4) | 40 ± 46 (–51,130) | –13 ± 11 (–34,8) | –3 ± 4 (–10,5) |
| 2P-3 | 0.97 | 0.94 | 0.97 | 1.00 |
| | 0 ± 8 (–17,16) | 17 ± 26 (–33,67) | –13 ± 11 (–34,9) | –3 ± 4 (–10,4) |
| 2P-4 | 0.98 | 0.98 | 0.97 | 1.00 |
| | –6 ± 7 (–20,8) | 9 ± 15 (–21,39) | –12 ± 11 (–34,9) | –3 ± 4 (–10,5) |
| 2P-5 | 0.98 | 0.99 | 0.97 | 1.00 |
| | –19 ± 7 (–33,–6) | 6 ± 12 (–18,30) | –12 ± 12 (–34,11) | –2 ± 4 (–10,5) |
| 3P-3 | 0.97 | 0.96 | 0.97 | 0.99 |
| | –11 ± 10 (–31,8) | –18 ± 23 (–62,26) | –10 ± 11 (–31,11) | 15 ± 14 (–12,42) |
| 3P-4 | 0.98 | 0.99 | 0.98 | 0.99 |
| | –8 ± 7 (–23,6) | –8 ± 13 (–33,18) | –9 ± 9 (–27,8) | 12 ± 13 (–13,38) |
| 3P-5 | 0.98 | 1.00 | 0.98 | 0.98 |
| | –7 ± 8 (–23,9) | –1 ± 8 (–16,15) | –9 ± 9 (–27,8) | 12 ± 13 (–14,38) |

Measured between each shortened T1 mapping scheme and MOLLI for native/postcontrast myocardial/blood T1 times. Data shown are as follows: first row, Pearson correlation coefficient as the *r*-value; second row, bias ± SD (95% limits of agreement) in msec. All *P*-values in Pearson correlation analysis are <0.0001.

approach resulted in a limited increase of spatial variability for native myocardial $T_1$ mapping by a factor of 1.2 when compared with MOLLI, and may thus be a valuable alternative for myocardial $T_1$ mapping, as the acquisition can be performed in just two heartbeats.

The proposed 2P model-based fitting technique enables correction for surface coil sensitivity variations using the normalization step of the dictionary matching. Exhaustive search-based optimization over the entire range of physiological myocardial and blood native/postcontrast $T_1$ times guarantees finding the global minimum of the cost function over a least-square optimization, and was successfully used with the 2P model. Although such an approach is more computationally intensive, the proposed GPU-based implementation substantially reduced the computation time to the subsecond scale per map, which is suitable for clinical application. Our results demonstrate that GPUs are particularly well suited for the reconstruction of $T_1$ maps. This finding is in good agreement with prior studies where GPU-based reconstruction substantially reduced the computation time of standard MOLLI reconstructions.[36] Further reduction of the computation time may be achieved using GPU cards with higher performance or advanced dictionary search approaches such as fast group matching algorithms.[37]

Although 2P-2 provides a 5-fold acceleration with respect to MOLLI, the overall acceleration rate in multislice protocols may be reduced by the required rest-periods between breath-holds. However, the repetition of two-heartbeat breath-holds may enable the use of shortened recovery periods, improve patient comfort, and increase the probability of successful breath-holds.

Bloch equations simulation was only performed on the employed inversion pulse to determine the inversion factor in the proposed 2P fitting model. However, Bloch equations simulation could also be used for the whole pulse sequence to generate the signal dictionary.[24–26] Such an approach could be used to model the effect of the 2D readouts and provide improved accuracy of the $T_1$ estimates, which will be the focus of future work.

In this work, the slice profile of the inversion pulses was approximated by one flip angle. Alternatively, the use of subslice-based simulations may improve the accuracy of the slice profile correction.[25] Estimation of the inversion factor could include a larger $B_0$ range if fatty tissues are considered. The use of a weighted average over the $B_0$ and $B_1$ ranges could also be considered to further improve the accuracy of the inversion factor estimates.

In this work, PSIR was employed for all reconstructions. Alternatively, a multifitting approach could have been used for all these reconstructions.[2] However, in our preliminary results (data not shown), we observed that the multifitting approach tended to fail to recover the correct signal

polarity for the 3P fitting model in the presence of short $T_1$ times. Although this technique was found robust for the 2P fitting model with all $T_1$ ranges, we decided to use the PSIR approach for uniformity consideration.

No in-plane motion correction was employed in this work. Image registration algorithms may provide different performance based on the amount and contrast of images used during the registration process. Therefore, to prevent such bias during in vivo evaluation of $T_1$ spatial variability and repeatability, we decided to discard the registration step of the reconstruction and discard datasets with inappropriate breath-hold. Nevertheless, retrospective image registration has been shown to improve the robustness of myocardial $T_1$ mapping.[38,39] Therefore, the design of tailored image registration algorithms for the proposed shortened $T_1$ mapping schemes will be the focus of future work. Finally, the use of shortened $T_1$ mapping schemes has the potential to improve the native registration of the $T_1$-weighted images in patients unable to sustain long stable breath-hold. This will be evaluated in future work in a larger patient cohort.

The evaluated shortened $T_1$ mapping schemes showed varying degrees of HR dependence. These results are aligned with previous studies that demonstrated the HR dependence of MOLLI $T_1$ times.[16,29,30] The proposed HR correction models were found successful in reducing HR-induced $T_1$ variation to <10 msec for the entire $T_1$ ranges. Alternative HR correction models have been proposed previously using a linear correction model based on measured $T_1$ and HR.[29,30] In those studies, the slope and offset of the linear correction were assumed to be $T_1$-independent. Although we showed that a linear relationship between HR and measured $T_1$ times is valid for a given $T_1$ range, the linear regression slope and offset are also $T_1$-dependent. Therefore, $T_1$-dependent correction models were found more accurate than a simple $T_1$-independent linear model.

The HR dependence of $T_1$ times is mainly due to the inaccuracies of the employed fitting models, partly caused by their $T_2$ dependence.[16] In this work, we found that the HR dependence of myocardial and blood $T_1$ times were different, which could be explained by their large $T_2$ difference (>150 msec vs. ~45 msec). Therefore, we decided to reconstruct two differently HR-corrected $T_1$ maps per slice: one with myocardium-based HR correction and one with blood-based HR correction. Automatic segmentation of the blood pool based on thresholding of $T_1$ maps has been previously proposed for ECV quantification.[40] Such an approach could allow the selection of the appropriate HR correction model on a per-voxel basis and may be used to generate a single HR corrected $T_1$ map for both the myocardium and blood.

This work has some limitations. First, the shortened $T_1$ mapping schemes have been evaluated from a subset of a conventional 5-(3)-3 MOLLI scheme. This choice was made to minimize the number of required breath-holds per subject. Second, the spatial variability measured as the SD over an ROI was used as a surrogate of the $T_1$ precision, as commonly reported in prior studies.[5,6,14,17] However, this approach is susceptible to partial volume effects as well as artifacts, and thus may not fully represent the impact of noise in $T_1$ time estimates. Third, trends were visually observed between MOLLI and the proposed shortened $T_1$ mapping schemes in terms of spatial variability and repeatability in phantom. However, the differences did not reach statistical significance, which may be due to insufficient statistical power related to the limited number of vials available in our phantom. Fourth, the patient study was based on a small cohort of consecutive patients referred for clinical cardiac MRI. The benefit of these techniques in a larger patient cohort including patients with breath-holding difficulties remains to be demonstrated and will be the focus of future studies. Furthermore, evaluation of this technique would be required in a cohort of patients with proven cardiac disease where mapping has clinical utility, such as with hypertrophic cardiomyopathy and Anderson-Fabry's disease.

In conclusion, the proposed two-heartbeat $T_1$ mapping scheme yields a 5-fold acceleration compared with MOLLI, with highly linearly correlated native/postcontrast myocardial/blood $T_1$ times, no significant difference of repeatability, and a limited spatial variability penalty at 1.5T. This approach may be a valuable alternative for myocardial $T_1$ mapping in patients with severe breath-holding difficulties and reduce examination time of multislice protocols.

## Acknowledgments

Contract grant sponsor: Health Innovation Challenge Fund; Contract grant number: HICF-R10-698; Contract grant sponsor: a parallel funding partnership between the Department of Health and the Wellcome Trust; Contract grant sponsor: Wellcome Engineering and Physical Sciences Research Council (EPSRC) Centre for Medical Engineering at King's College London; Contract grant number: WT 203148/Z/16/Z; Contract grant sponsor: EPSRC; Contract grant number: EP/R010935/1; Contract grant sponsor: National Institute for Health Research (NIHR) Biomedical Research Centre award to Guy's and St Thomas' National Health Service (NHS) Foundation Trust in partnership with King's College London; Contract grant sponsor: NIHR Healthcare Technology Co-operative for Cardiovascular Disease at Guy's and St Thomas' NHS Foundation Trust; Contract grant sponsor: UK Medical Research Council; Contract grant number: MR/P01979X/1 (to M.S.N.).

## References

1. Moon JC, Messroghli DR, Kellman P, et al.; Society for Cardiovascular Magnetic Resonance I, Cardiovascular Magnetic Resonance Working Group of the European Society of C. Myocardial T1 mapping and

extracellular volume quantification: A Society for Cardiovascular Magnetic Resonance (SCMR) and CMR Working Group of the European Society of Cardiology consensus statement. J Cardiovasc Magn Reson 2013; 15:92.

2. Messroghli DR, Radjenovic A, Kozerke S, Higgins DM, Sivananthan MU, Ridgway JP. Modified Look-Locker inversion recovery (MOLLI) for high-resolution T1 mapping of the heart. Magn Reson Med 2004;52:141–146.
3. Arheden Hk, Saeed M, Higgins CB, et al. Measurement of the distribution volume of gadopentetate dimeglumine at echo-planar MR imaging to quantify myocardial infarction: Comparison with 99mTc-DTPA autoradiography in rats. Radiology 1999;211:698–708.
4. Wong TC, Piehler K, Meier CG, et al. Association between extracellular matrix expansion quantified by cardiovascular magnetic resonance and short term mortality. Circulation 2012:CIRCULATIONAHA. 111.089409.
5. Piechnik SK, Ferreira VM, Dall'Armellina E, et al. Shortened modified Look-Locker inversion recovery (ShMOLLI) for clinical myocardial T1-mapping at 1.5 and 3 T within a 9 heartbeat breathhold. J Cardiovasc Magn Reson 2010;12:69.
6. Weingärtner S, Roujol S, Akçakaya M, Basha TA, Nezafat R. Free-breathing multislice native myocardial T1 mapping using the slice-interleaved T1 (STONE) sequence. Magn Reson Med 2015;74:115–124.
7. Chow K, Flewitt JA, Green JD, Pagano JJ, Friedrich MG, Thompson RB. Saturation recovery single-shot acquisition (SASHA) for myocardial T (1) mapping. Magn Reson Med 2014;71:2082–2095.
8. Higgins DM, Ridgway JP, Radjenovic A, Sivananthan UM, Smith MA. T1 measurement using a short acquisition period for quantitative cardiac applications. Med Phys 2005;32:1738–1746.
9. Fitts M, Breton E, Kholmovski EG, et al. Arrhythmia insensitive rapid cardiac T1 mapping pulse sequence. Magn Reson Med 2013;70: 1274–1282.
10. Song T, Stainsby JA, Ho VB, Hood MN, Slavin GS. Flexible cardiac T1 mapping using a modified Look-Locker acquisition with saturation recovery. Magn Reson Med 2012;67:622–627.
11. Slavin GS, Stainsby JA. True T1 mapping with SMART 1 Map (saturation method using adaptive recovery times for cardiac T 1 mapping): A comparison with MOLLI. J Cardiovasc Magn Reson 2013;15:P3.
12. Weingartner S, Akcakaya M, Basha T, et al. Combined saturation/-inversion recovery sequences for improved evaluation of scar and diffuse fibrosis in patients with arrhythmia or heart rate variability. Magn Reson Med 2014;71:1024–1034.
13. Akçakaya M, Weingärtner S, Basha TA, Roujol S, Bellm S, Nezafat R. Joint myocardial T1 and T2 mapping using a combination of saturation recovery and T2-preparation. Magn Reson Med 2016;76:888–896.
14. Roujol S, Weingärtner S, Foppa M, et al. Accuracy, precision, and reproducibility of four T1 mapping sequences: A head-to-head comparison of MOLLI, ShMOLLI, SASHA, and SAPPHIRE. Radiology 2014;272:683–689.
15. Teixeira T, Hafyane T, Stikov N, Akdeniz C, Greiser A, Friedrich MG. Comparison of different cardiovascular magnetic resonance sequences for native myocardial T1 mapping at 3T. J Cardiovasc Magn Reson 2016; 18:65.
16. Kellman P, Hansen MS. T1-mapping in the heart: Accuracy and precision. J Cardiovasc Magn Reson 2014;16:2.
17. Weingärtner S, Meßner NM, Budjan J, et al. Myocardial T 1-mapping at 3T using saturation-recovery: Reference values, precision and comparison with MOLLI. J Cardiovasc Magn Reson 2017;18:84.
18. Chow K, Flewitt J, Pagano JJ, Green JD, Friedrich MG, Thompson RB. T 2-dependent errors in MOLLI T 1 values: Simulations, phantoms, and in-vivo studies. J Cardiovasc Magn Reson 2012;14:P281.
19. Robson MD, Piechnik SK, Tunnicliffe EM, Neubauer S. T1 measurements in the human myocardium: The effects of magnetization transfer on the SASHA and MOLLI sequences. Magn Reson Med 2013;70:664–670.
20. Kellman P, Herzka DA, Hansen MS. Adiabatic inversion pulses for myocardial T1 mapping. Magn Reson Med 2014;71:1428–1434.
21. Deichmann R, Haase A. Quantification of T1 values by SNAPSHOT-FLASH NMR imaging. J Magn Reson 1992;96:608–612.
22. Xue H, Greiser A, Zuehlsdorff S, et al. Phase-sensitive inversion recovery for myocardial T1 mapping with motion correction and parametric fitting. Magn Reson Med 2013;69:1408–1420.
23. Shao J, Nguyen KL, Natsuaki Y, Spottiswoode B, Hu P. Instantaneous signal loss simulation (InSiL): An improved algorithm for myocardial T (1) mapping using the MOLLI sequence. J Magn Reson Imaging 2015; 41:721–729.
24. Marty B, Vignaud A, Greiser A, Robert B, de Sousa PL, Carlier PG. BLOCH equations-based reconstruction of myocardium t1 maps from modified Look-Locker inversion recovery sequence. PLoS One 2015;10: e0126766.
25. Shao J, Rapacchi S, Nguyen KL, Hu P. Myocardial T1 mapping at 3.0 tesla using an inversion recovery spoiled gradient echo readout and bloch equation simulation with slice profile correction (BLESSPC) T1 estimation algorithm. J Magn Reson Imaging 2016;43:414–425.
26. Xanthis CG, Bidhult S, Kantasis G, Heiberg E, Arheden H, Aletras AH. Parallel simulations for QUAntifying RElaxation magnetic resonance constants (SQUAREMR): An example towards accurate MOLLI T1 measurements. J Cardiovasc Magn Reson 2015;17:104.
27. Marks B, Mitchell DG, Simelaro JP. Breath-holding in healthy and pulmonary-compromised populations: Effects of hyperventilation and oxygen inspiration. J Magn Reson Imaging 1997;7:595–597.
28. Lourakis M. levmar: Levenberg-Marquardt nonlinear least squares algorithms in C/C++. 2004; http://www.ics.forth.gr/~lourakis/levmar/
29. Messroghli DR, Plein S, Higgins DM, et al. Human myocardium: Single-breath-hold MR T1 mapping with high spatial resolution—reproducibility study. Radiology 2006;238:1004–1012.
30. Messroghli DR, Walters K, Plein S, et al. Myocardial T1 mapping: Application to patients with acute and chronic myocardial infarction. Magn Reson Med 2007;58:34–40.
31. Cerqueira MD, Weissman NJ, Dilsizian V, et al.; American Heart Association Writing Group on Myocardial S, Registration for Cardiac I. Standardized myocardial segmentation and nomenclature for tomographic imaging of the heart. A statement for healthcare professionals from the Cardiac Imaging Committee of the Council on Clinical Cardiology of the American Heart Association. Circulation 2002;105:539–542.
32. Chow K, Yang Y, Shaw P, Kramer CM, Salerno M. Robust free-breathing SASHA T1 mapping with high-contrast image registration. J Cardiovasc Magn Reson 2016;18:47.
33. Akçakaya M, Weingärtner S, Roujol S, Nezafat R. On the selection of sampling points for myocardial T1 mapping. Magn Reson Med 2015;73: 1741–1753.
34. Kellman P, Xue H, Chow K, Spottiswoode BS, Arai AE, Thompson RB. Optimized saturation recovery protocols for T1-mapping in the heart: Influence of sampling strategies on precision. J Cardiovasc Magn Reson 2014;16:55.
35. Hong K, Kim D. MOLLI and AIR T1 mapping pulse sequences yield different myocardial T1 and ECV measurements. NMR Biomed 2014;27: 1419–1426.
36. Liu S, Bustin A, Burshka D, Menini A, Odille F. GPU implementation of Levenberg-Marquardt optimization for T1 mapping. Computing 2017; 44:1.
37. Cauley SF, Setsompop K, Ma D, et al. Fast group matching for MR fingerprinting reconstruction. Magn Reson Med 2015;74:523–528.
38. Xue H, Shah S, Greiser A, et al. Motion correction for myocardial T1 mapping using image registration with synthetic image estimation. Magn Reson Med 2012;67:1644–1655.
39. Roujol S, Foppa M, Weingartner S, Manning WJ, Nezafat R. Adaptive registration of varying contrast-weighted images for improved tissue characterization (ARCTIC): Application to T1 mapping. Magn Reson Med 2015;73:1469–1482.
40. Kellman P, Wilson JR, Xue H, Ugander M, Arai AE. Extracellular volume fraction mapping in the myocardium. Part 1: Evaluation of an automated method. J Cardiovasc Magn Reson 2012;14:63.